A Physics-Based Empirical Model of Dynamic I_{OFF} Under Switching Operation in *p*-GaN Gate Power HEMTs

Yuru Wang, Tao Chen, Mengyuan Hua, *Member, IEEE*, Jin Wei, *Member, IEEE*, Zheyang Zheng, Wenjie Song, Song Yang, Kailun Zhong, and Kevin J. Chen, *Fellow, IEEE*

***Abstract*—In this article, an empirical model of dynamic OFF-state leakage current (I_{OFF}) under switching operation in *p*-GaN gate high-electron-mobility transistors is established based on its underlying physical mechanism. The impacts of relevant switching conditions, including switching frequency, duty cycle, OFF-state delay time, gate drive voltage, and temperature are all considered in the modeling of dynamic I_{OFF}. A good agreement between the modeled dynamic I_{OFF} and experimental results is achieved. Based on this model, the OFF-state power consumption (E_{OFF}) and OFF/ON-state power consumption ratio ($E_{\mathrm{OFF}}/E_{\mathrm{ON}}$) under dynamic switching operation can be predicted for various switching conditions. As the device worked at a high switching frequency (e.g., 1 MHz and duty cycle: 50%) with a gate drive voltage of 7 V and temperatures from 25 to 150 °C, the $E_{\mathrm{OFF}}/E_{\mathrm{ON}}$ ratio is calculated from 0.53% to 0.07%, which is three to two orders of magnitude higher than what is projected from static OFF-state current characteristics.**

***Index Terms*—Dynamic $\mathrm{I_{OFF}}$, empirical model, *p*-GaN gate HEMT, physics-based.**

I. Introduction

GaN-based high-electron-mobility transistors (HEMTs), with their superior device properties, have gained increasing attention in the next-generation high-frequency, high-power-density, and high-efficiency power switching systems [1]–[3]. To be accepted in the market, normally OFF operation is of critical importance for the fail-safe operation and simplified gate drive topology [3]. Among several normally-OFF technologies [4]–[7], the *p*-GaN gate solution is a mainstream in the commercial GaN-based power device market with a good balance among performance, reliability, and cost [8]–[10]. Two types of gate contact between the gate metal and *p*-GaN layer are currently adopted in the commercial products, i.e., Ohmic-type [11] and Schottky-type [16]. The Ohmic-type *p*-GaN gate HEMT has been developed under the concept of gate injection transistor and has presented impressive performance [12] and reliability [13]. A Schottky-type gate contact to the *p*-GaN layer is the other approach for the merits of reduced gate leakage current and a larger gate swing [14]–[18].

Apart from the distinct gate characteristics, critical parameters of currently available *p*-GaN gate HEMTs are subject to the influence of various trapping effects under dynamic operation conditions. In order to better understand and further predict the device behaviors in power switching circuits, it is necessary to characterize the device's performance under dynamic operation conditions.

Extensive investigation has been carried out to understand and reduce the current collapse-induced dynamic ON-resistance (R_{ON}) degradation in GaN-on-Si power HEMTs [12], [19]–[22]. Besides, in Schottky-type *p*-GaN gate HEMT, because the *p*-GaN layer is a "floating region" without a direct electrical connection to any of the transistor's three terminals, a drain-bias-induced dynamic positive shift of threshold voltage (V_{TH}) would occur during switching operation [15], [23]. A sufficiently large gate turn-ON voltage should be applied to overdrive this device and overcome the V_{TH}-shift-induced dynamic R_{ON} degradation in practical power switching applications.

For the OFF-state characteristics, an important application-relevant device dynamic behavior—dynamic OFF-state leakage current (I_{OFF})—has been revealed in *p*-GaN gate HEMTs [24], [25]. It is found that the I_{OFF} under dynamic pulse-mode operation is higher than the I_{OFF} obtained in the quasi-static measurement, and it is further enhanced with the ON-state hole injection from the gate. The impacts of relevant switching conditions, such as switching frequency, duty cycle, gate drive voltage, and temperature on dynamic I_{OFF}, were analyzed, and the corresponding qualitative physical explanations were provided [25]. The accurate modeling of dynamic I_{OFF} could provide the accurate estimation of OFF-state power consumption (E_{OFF}) and OFF/ON-state power consumption ratio ($E_{\mathrm{OFF}}/E_{\mathrm{ON}}$) in practical power switching circuits and systems.

Manuscript received December 24, 2020; accepted February 22, 2021. Date of publication February 26, 2021; date of current version June 1, 2021. This work was supported in part by Hong Kong Innovation and Technology Fund under Grant ITS/412/17FP and in part by the Research Impact Fund under Grant R6008-18. Recommended for publication by Associate Editor M. Nawaz. *(Corresponding author: Kevin J. Chen.)*

Yuru Wang, Tao Chen, Zheyang Zheng, Wenjie Song, Song Yang, Kailun Zhong, and Kevin J. Chen are with the Department of Electronic and Computer Engineering, The Hong Kong University of Science and Technology, Hong Kong 999077, China (e-mail: ywangfk@connect.ust.hk; tchenaw@connect.ust.hk; zzhengah@connect.ust.hk; wsongab@connect.ust.hk; syangaj@connect.ust.hk; kzhongac@connect.ust.hk; eekjchen@ust.hk).

Mengyuan Hua is with the Department of Electrical and Electronic Engineering, The Southern University of Science and Technology, Shenzhen 518000, China (e-mail: huamy@sustech.edu.cn).

Jin Wei is with the Institute of Microelectronics, Peking University, Beijing 100871, China (e-mail: jweiaf@connect.ust.hk).

Color versions of one or more figures in this article are available at https://doi.org/10.1109/TPEL.2021.3062450.

Digital Object Identifier 10.1109/TPEL.2021.3062450

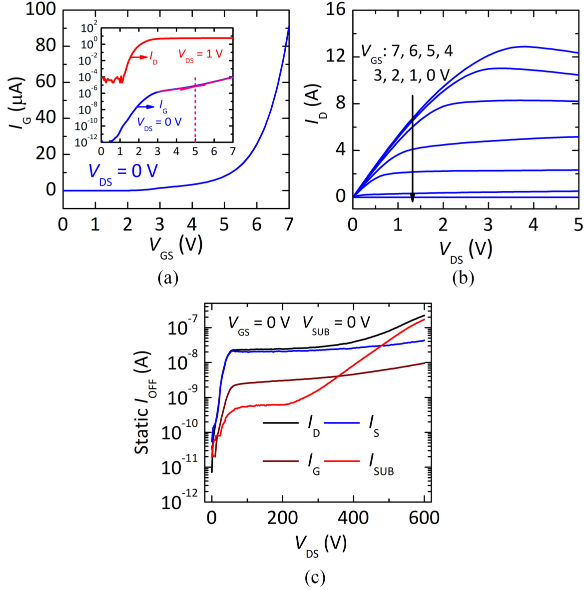

Fig. 1. Static *I–V* characteristics of a Schottky-type *p*-GaN gate HEMT. (a) Forward I_G–V_{GS} characteristics. Inset: Semilog plot of I_G–V_{GS} ($V_{DS} = 0$ V) and I_D–V_{GS} ($V_{DS} = 1$ V). (b) Output characteristics. (c) Quasi-static $I_{\rm OFF}$–V_{DS} characteristics with a gate bias of 0 V. The Si substrate is grounded.

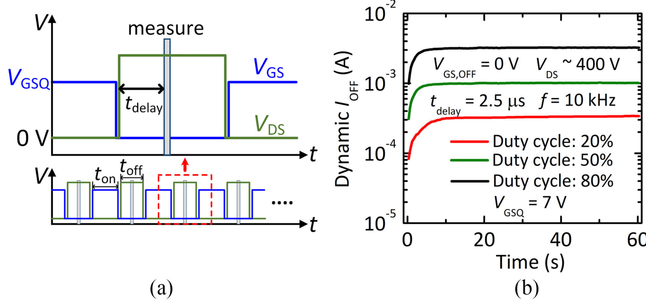

Fig. 2. (a) Waveforms of continuous soft-switching terminal voltages from a pulsed *I–V* system for the measurement of dynamic $I_{\rm OFF}$. (b) Time-resolved dynamic $I_{\rm OFF}$ under the corresponding continuous soft-switching conditions.

In this article, we present an empirical model of dynamic $I_{\rm OFF}$ under switching operation for the Schottky-type *p*-GaN gate HEMT. The model is established based on the physical understandings with the considerations of key switching conditions, such as switching frequency, duty cycle, OFF-state delay time, ON-state gate drive voltage, and temperature. A good agreement between the modeled and measured results of dynamic $I_{\rm OFF}$ is achieved. This model facilitates the quantitative projections of $E_{\rm OFF}$ and $E_{\rm OFF}/E_{\rm ON}$ ratio under dynamic switching operation, providing valuable guidance to quantify the impact of dynamic $I_{\rm OFF}$, especially in the high-frequency power switching applications.

This article is organized as follows. Section II describes the physical mechanisms of $I_{\rm OFF}$ under static and dynamic conditions in *p*-GaN gate HEMTs. A physics-based empirical model of dynamic $I_{\rm OFF}$ under switching operation is presented in Section III. The corresponding results and discussion are further shown in Section IV. Finally, the conclusion is drawn in Section V.

II. Physical Mechanisms of $I_{\rm OFF}$ Under Static and Dynamic Conditions

The device used in this work is commercially available 650-V/7.5-A *p*-GaN gate HEMTs from GaN systems [26]. The transfer ($V_{DS} = 1$ V) and I_G-V_{GS} ($V_{DS} = 0$ V) curves are plotted in Fig. 1(a). The device features a $V_{\rm TH}$ of 1.35 V (at $V_{DS} = 1$ V and $I_D = 1$ mA) with normally OFF operation. The forward ON-state I_G is $\sim$91 μA at V_{GS} of 7 V and the I_D/I_G ratio is about 10^5, which is attributed to the reverse-biased metal/*p*-GaN Schottky junction [27]. A transition at V_{GS} in the I_G-V_{GS} curve can be identified. This is the turn-ON voltage of the gate hetero p-n junction and the commencement of the ON-state hole injection [28]. From the output curves [see Fig. 1(b)], the static $R_{\rm ON}$ is around 190 mΩ (at $V_{GS} = 7$ V, $V_{DS} = 1$ V, yielding an ON-state current ($I_{\rm ON}$) of 5.26 A). For the quasi-static $I_{\rm OFF}$, the OFF-state drain leakage is mainly dominated by the lateral drain-to-source leakage current when the drain bias ranges between 0 and 400 V and starts to be dominated by the vertical drain-to-substrate leakage current when the drain bias exceeds 400 V, as shown in Fig. 1(c). The quasi-static $I_{\rm OFF}$ ($I_{{\rm OFF},S}$) is $\sim$40 nA at V_{DS} of 400 V and the $I_{\rm ON}/I_{{\rm OFF},S}$ ratio is more than 10^8.

Aiming at evaluating the dynamic $I_{\rm OFF}$ under practical switching operations, the ac voltage signals with continuous soft-switching waveforms were generated and applied to the device using a high-speed AMCAD pulsed *I–V* system, as shown in Fig. 2(a). During each switching cycle, the device was first stressed in the ON-state with a forward gate bias of V_{GSQ} and then switched to the OFF-state with a preset measurement delay time ($t_{\rm delay}$) for dynamic $I_{\rm OFF}$ measurement. The pulsed OFF-state V_{DS} was varied within a narrow range from 398 to 400 V to mimic continuous switching at V_{DS} $\sim$400 V. Under the continuous soft switching specified above, dynamic $I_{\rm OFF}$ increases first and then saturates at a certain level after some numbers of switching cycles ($\sim$10 s), as shown in Fig. 2(b).

The mechanisms that govern the static and dynamic $I_{\rm OFF}$ are depicted in Fig. 3. Under the thermal equilibrium, the buffer traps are only filled partially [29]. In the OFF-state, the electrons are injected from the source to the buffer. In a quasi-static measurement, the pre-empty traps are gradually filled by electrons injected from the source to the buffer, as V_{DS} is slowly increased. The slow ramping rate allows sufficient time for the empty traps to capture electrons, leading to the increased negative space charges [see Fig. 3(a)]. The additional negative space charges in the buffer layer (in the forms of ionized acceptor traps or neutral donor traps) play the role of raising the energy barrier in the leakage path and blocking the leakage current in the static OFF-state [29]–[31]. Under switching operation with a sufficiently large forward gate bias (i.e., gate overdrive) in the ON-state, holes can be injected from the *p*-GaN layer to the two-dimensional electron gas (2DEG) channel. These holes could either recombine with electrons in the channel to emit photons of 3.4 eV and pump electrons from the buffer traps [32], [33] or further transport to compensate the buffer traps with electrons [12]. Both processes could lead to the reduced

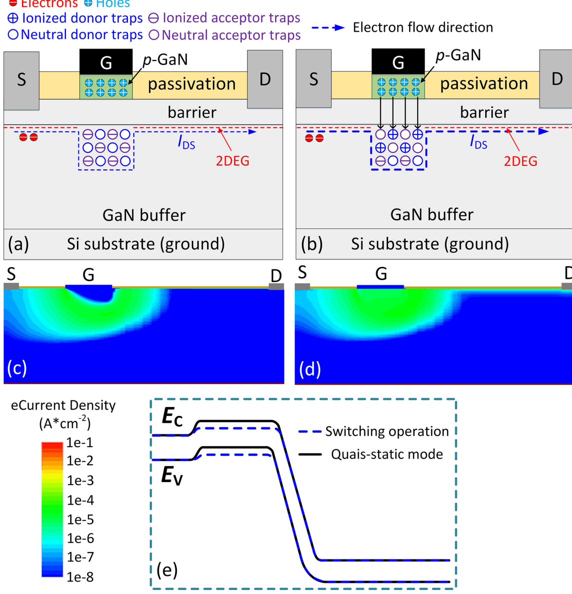

Fig. 3. Schematic cross sections for explaining the static and dynamic I_{OFF} in p-GaN gate HEMT. (a) Quasi-static mode. (b) Switching operation. TCAD-simulated distribution profile of OFF-state electron current density under (c) quasi-static condition and (d) switching operation. (e) Energy band diagrams under the channel in quasi-static condition and switching operation. In the gate-to-source and gate-to-drain access regions, the leakage current flows through the 2DEG channel at the barrier/GaN heterointerface, as indicated in (a) and (b).

TABLE I
KEY PHYSICAL PARAMETERS USED IN SIMULATION

Physical parameter	Value
Al composition in AlGaN layer	0.15
Thickness of AlGaN layer	15 nm
Thickness of p-GaN layer	100 nm
Activated Mg concentration in p-GaN layer	2×10^{18} cm^{-3}
Ionization barrier of Mg doping	186 meV
Hole concentration at room temperature	2×10^{17} cm^{-3}
Gate Schottky barrier height	1.3 eV [16]
Donor-like traps in GaN buffer	E_c - 0.6 eV, 2×10^{16} cm^{-3} [29]
Acceptor-like traps in GaN buffer	E_v + 0.9 eV, 1×10^{18} cm^{-3} [37]

negative space charges under the gate in the buffer [see Fig. 3(b)]. As the device is switched to the OFF-state, the hole injection is turned OFF, while the ionized traps would persist for a period of time before recapturing electrons [34]–[36], leading to a lowered energy barrier under the channel with increased dynamic I_{OFF} [see Fig. 3(e)].

Technology computer aided design (TCAD)-based numerical simulation was performed using Synopsys software to reveal the differences in I_{OFF} under the quasi-static and dynamic switching conditions [see Fig. 3(c) and (d)]. The key physical parameters of simulated device structure are illustrated in Table I. Electron/hole continuity equations and Poisson equation are solved self-consistently in the simulation. Shockley–Read–Hall recombination, Auger recombination, Radiative recombination, incomplete dopant ionization, doping-dependent transport, thermionic emission, tunneling, Poole–Frenkel emission, band narrowing, and impact ionization are all taken into account.

Under dynamic switching operation, a much broader lateral leakage path around the depleted channel can be induced by the ON-state hole injection, resulting in a higher dynamic I_{OFF} [see Fig. 3(d)].

A continuous reduction of negative space charges by the injected holes in each cycle under switching operation leads to an increase of dynamic I_{OFF}. After certain number of switching cycles, a steady state is reached when the rate of reduced electrons in the buffer traps by the injected holes from the p-GaN gate during the ON-state balances out the rate of recapturing electrons facilitated by the leakage current during the OFF-state. Such a balance results in a stable barrier to electron flow in the leakage path of buffer and the stabilization of dynamic I_{OFF} [see Fig. 2(b)].

The saturated high dynamic I_{OFF} with hole injection is dominated by the lateral drain-to-source leakage current and is determined by the energy barrier height under the gate [25]. A lower energy barrier under the gate could enhance electron emission from source to drain that leads to a higher dynamic I_{OFF}. The barrier height under the gate is related to the number of reduced negative space charges in the buffer, which is impacted by both the detrapping (i.e., removal of trapped electrons by holes) process in the ON-state and the trapping (i.e., recapturing electrons for the ionized traps) process in the OFF-state.

With a larger t_{delay}, more electrons could be recaptured in the buffer and a smaller dynamic I_{OFF} is obtained. A larger duty cycle under the same switching frequency (f) leads to a longer ON-state duration time (t_{on}) with stronger hole injection and a shorter OFF-state time (t_{off}) with a weaker electron-recapturing process in each cycle. Thus, the dynamic I_{OFF} becomes larger with a larger duty cycle [see Fig. 2(b)]. As larger V_{GSQ} leads to stronger hole injection into the channel and buffer, more electrons would be pumped out of or released from traps, resulting in a higher dynamic I_{OFF}. The increased ambient temperature (T) would accelerate the electron-recapturing process in the OFF-state, leading to a lower dynamic I_{OFF} at higher temperatures.

In the following sections, we would focus on the influences of t_{delay}, t_{on}, t_{off}, V_{GSQ}, and T on dynamic I_{OFF}. The experimental section is based on the measurement results of dynamic I_{OFF} by using the high-speed AMCAD pulsed I--V system with fast continuous switching waveforms [see Fig. 2(a)]. The pulsed I–V system could generate relatively smooth waveforms without oscillations. The saturated value of dynamic I_{OFF} after a certain number of switching cycles (∼10 s) is extracted for the model establishment. The switching frequency (f) is set to be $1/(t_{\mathrm{on}}+t_{\mathrm{off}})$ and the duty cycle (D) is $t_{\mathrm{on}}/(t_{\mathrm{on}}+t_{\mathrm{off}})$. The empirical model of dynamic I_{OFF} will be developed based on the physical understandings described in this section.

III. PHYSICS-BASED EMPIRICAL MODEL OF DYNAMIC I_{OFF} UNDER SWITCHING OPERATION

A. Influence of Measurement Delay Time

The quiescent ON-state gate bias V_{GSQ} is first set at 7 V in the model development to assure adequate yet safe gate overdrive [26]. During the ON-state of each switching cycle, holes are injected from the p-GaN gate to the underneath channel and

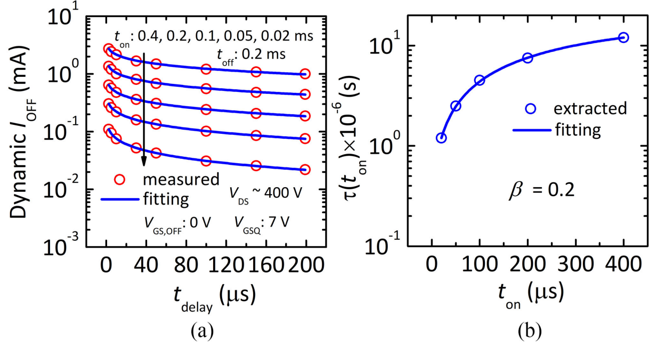

Fig. 4. (a) Dynamic I_{OFF} versus t_{delay} with different t_{on}. (b) Extracted time constant τ as a function of t_{on}. The solid lines are fitting curves.

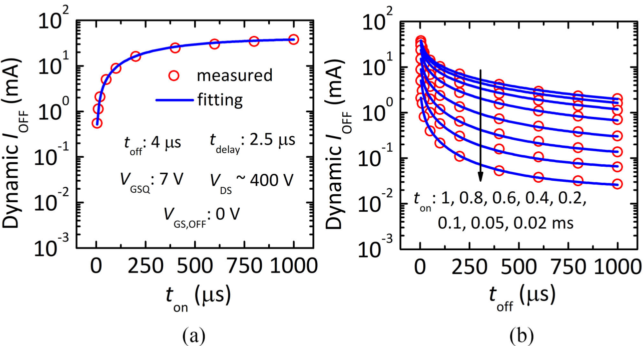

Fig. 5. (a) Dynamic I_{OFF} versus t_{on}. (b) Dynamic I_{OFF} versus t_{off} with different t_{on}. The solid lines are fitting curves.

buffer layer, resulting in partial removal of trapped electrons in the buffer layer below the channel. As the device is switched to the OFF-state, the hole injection is turned OFF immediately, while the ionized trap centers would be gradually filled with electrons due to the limited recapturing rate of the traps [34]–[36]. With a longer t_{delay}, dynamic I_{OFF} is reduced as more electrons can be effectively recaptured by the buffer traps. The larger number of recaptured electrons would result in a raised barrier in the leakage path and reduced recapturing rate in the OFF-state. As a result, the dynamic I_{OFF} ($I_{\mathrm{OFF},D}$) versus t_{delay} follows a stretched-exponential decay law [36]

$$I_{\mathrm{OFF},\ D}\ \ (t_{\mathrm{delay}}) = I_{\mathrm{OFF},\ D}\ \ (0)\exp\left[-\left(\frac{t_{\mathrm{delay}}}{\tau}\right)^{\beta}\right] \tag{1}$$

where $I_{\mathrm{OFF},D}$ (0) is the value of dynamic I_{OFF} at the moment of switching OFF the hole injection, τ is the time constant for the ionized traps to recapture electrons in the OFF-state, and β is the decay exponent. As the minimum measurement delay time is 2.5 μs in the pulsed *I–V* system, we started the fitting point with $t_{\mathrm{delay}} = 2.5\ \mu$s by

$$I_{\mathrm{OFF},\ D}\ \ (t_{\mathrm{delay}}) \ = \ I_{\mathrm{OFF},\ D}\ (2.5\ \mu\mathrm{s}) \times \exp\left[-\left(\frac{t_{\mathrm{delay}}}{\tau}\right)^{\beta} + \left(\frac{2.5\ \mu\mathrm{s}}{\tau}\right)^{\beta}\right]. \tag{2}$$

It is found that the dynamic I_{OFF} decay with t_{delay} after the ON-state hole injection at the given t_{on}, t_{off}, and V_{GSQ} could be fitted well with a stretched-exponential equation, as shown in Fig. 4(a). The fitting parameter of β is 0.2 and the time constant τ is a function of t_{on} [see Fig. 4(b)]. A smaller τ implies a larger recapturing rate for the ionized traps in the OFF-state. With a shorter t_{on} in each cycle, less holes would be injected into the region below the 2DEG channel, where the trapped electrons, which are closer to the channel, would be ionized at first. These ionized traps would be easier to recapture electrons from the 2DEG in the source side due to the relatively shorter space distance, resulting in a larger recapturing rate. A fitting function of τ about t_{on} is provided as follows:

$$\tau \ = \ \tau\ (t_{\mathrm{on}}) = \tau_0\ - \tau_1 \exp\left(-\frac{t_{\mathrm{on}}}{\tau_2}\right). \tag{3}$$

B. Dependence of Dynamic I_{OFF} on the ON-State Duration Time

Under practical switching operation with continuous waveforms, dynamic I_{OFF} is saturated due to a balanced trapping/detrapping process of buffer traps in each switching cycle. The saturated value of dynamic I_{OFF} is related to the number of ionized buffer traps at the balanced level, which is influenced by the switching frequency and duty cycle. As a result, the starting point of fitting [i.e., $I_{\mathrm{OFF},D}$ (2.5 μs)] in each cycle is a function of t_{on} and t_{off}, given by

$$I_{\mathrm{OFF,D}}\ (2.5\ \mu\mathrm{s}) = I\ (t_{\mathrm{on}},\ t_{\mathrm{off}},\ t_{\mathrm{delay}}) = I\ (t_{\mathrm{on}},\ t_{\mathrm{off}},\ 2.5\ \mu\mathrm{s})\,. \tag{4}$$

This fitting was established with a fixed t_{delay} of 2.5 μs to identify the dependence of $I_{\mathrm{OFF},D}$ (2.5 μs) on t_{on} and t_{off}. First, we started the fitting with a fixed t_{off} of 4 μs (the minimum pulsewidth of OFF-state). With fixed t_{off} and t_{delay}, dynamic I_{OFF} at the balanced level would increase with longer t_{on} that results in larger number of holes injected to the buffer at ON-state in each cycle. The more there are injected holes, the more buffer traps would be ionized. The number of ionized traps with the increase of t_{on} would gradually be saturated as a result of the reduced unionized electron traps in the buffer layer under the gate. As a result, the dynamic I_{OFF} versus t_{on} follows a complementary exponential function. The measurement data could be well fitted by the following equation, as shown in Fig. 5(a):

$$I\ \ (t_{\mathrm{on}},\ 4\ \mu\mathrm{s},\ 2.5\ \mu\mathrm{s}) = A_1\ \ - A_1 \exp\left(-\frac{t_{\mathrm{on}}}{B_1}\right) \tag{5}$$

where A_1 (unit: *A*) is the value of dynamic I_{OFF} when the number of ionized electron traps reaches its saturation with the certain levels of ON-state hole injection and OFF-state recapturing process (e.g., $V_{GSQ} = 7$ V, $t_{\mathrm{off}} = 4\ \mu$s, and $t_{\mathrm{delay}} = 2.5\ \mu$s). B_1 is the fitting parameter (unit: *s*) associated with the ON-state detrapping process (i.e., ionization of electrons from traps).

C. Dependence of Dynamic I_{OFF} on the OFF-State Recapturing Time

With the increase of t_{off} for a given t_{on} and t_{delay}, dynamic I_{OFF} at the balanced level decreases due to the enhanced recapturing electron process in the OFF-state for each cycle. The longer the t_{off} is, the more electrons can be recaptured in each cycle,

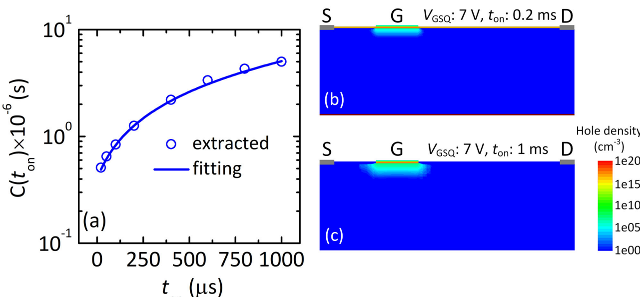

Fig. 6. (a) Extracted parameter of C as a function of $t_{\rm on}$. Simulated hole density distribution profile with (b) $t_{\rm on} = 0.2$ ms and (c) $t_{\rm on} = 1$ ms ($V_{GSQ} = 7$ V).

leading to the reduced ionized traps in the buffer at the balanced level. The reducing rate of dynamic $I_{\rm OFF}$ with the increase of $t_{\rm off}$ would gradually be slower due to the reduced recapturing rate in the OFF-state with a diminishing number of ionized traps. So, the dynamic $I_{\rm OFF}$ versus $t_{\rm off}$ follows a stretched-exponential decay law [see Fig. 5(b)]. Because the minimum OFF-state recapturing time $t_{\rm off}$ in the measurement setup is 4 μs, we fit the dynamic $I_{\rm OFF}$ versus $t_{\rm off}$ by

$$
\begin{aligned}
I(t_{\rm on}, t_{\rm off}, 2.5\,\mu{\rm s}) &= I(t_{\rm on}, 4\,\mu{\rm s}, 2.5\,\mu{\rm s}) \\
&\quad * \exp\left[-\left(\frac{t_{\rm off}}{C}\right)^{D_1} + \left(\frac{4\,\mu{\rm s}}{C}\right)^{D_1}\right] + I_0 \\
I_0 &= A_2 \ * I\left(t_{\rm on},\ 4\,\mu{\rm s},\ 2.5\,\mu{\rm s}\right) \qquad (6)
\end{aligned}
$$

where I ($t_{\rm on}$, 4 μs, 2.5 μs) is the function about dynamic $I_{\rm OFF}$ versus $t_{\rm on}$ with a fixed $t_{\rm off}$ of 4 μs and $t_{\rm delay}$ of 2.5 μs [i.e., (5)]. C is the fitting parameter (unit: s) associated with the recapturing process in the OFF-state, and D_1 is the decay exponent. I_0 represents the current when all the ionized traps are recovered with long enough $t_{\rm off}$, when only one cycle of hole injection could lead to a value of dynamic $I_{\rm OFF}$ at a certain $t_{\rm delay}$. The model based on (6) can very well fit the measured dynamic $I_{\rm OFF}$ as a function $t_{\rm off}$, as shown in Fig. 5(b).

It is found that the fitting parameter C is also a function of $t_{\rm on}$ [see Fig. 6(a)], as extracted from the fitting curves in Fig. 5(b). A smaller C implies a larger recapturing rate for the ionized traps in the OFF-state with a certain period of $t_{\rm off}$. With a shorter $t_{\rm on}$, there are less holes injected to the buffer region under the gate, as indicated by the hole density distribution profiles from TCAD simulation [see Fig. 6(b) and (c)]. Thus, only the traps closer to the channel are deionized or detrapped. As these empty traps are physically closer to the 2DEG channel of the access region on the source side, it is easier for them to recapture electrons at the OFF-state, resulting in a larger recapturing rate. With longer $t_{\rm on}$, more holes are injected and penetrate deeper into the buffer for detrapping [see Fig. 6(c)]. When it comes to electron trapping under high-drain-bias OFF-state, the deeper traps would effectively exhibit a longer recapture time, as they are physically further away from the source of electrons (i.e., the 2DEG channel in the access regions).

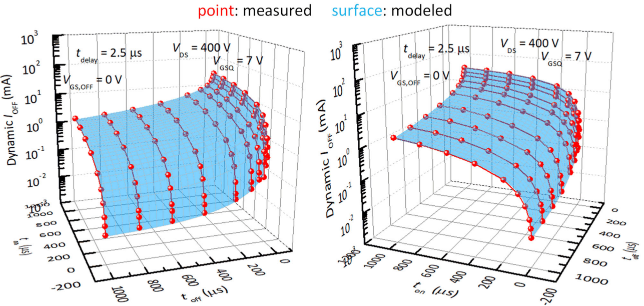

Fig. 7. Measured and modeled $I_{{\rm OFF},D}$ (2.5 μs) versus $t_{\rm on}$ and $t_{\rm off}$.

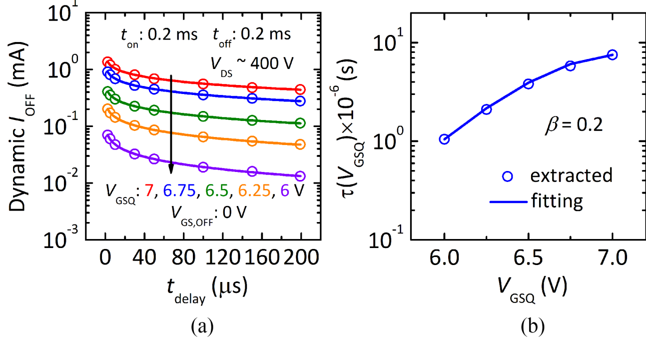

Fig. 8. (a) Dynamic $I_{\rm OFF}$ versus $t_{\rm delay}$ with different V_{GSQ}. (b) Extracted time constant τ as a function of V_{GSQ}. The solid lines are fitting curves.

A fitting function of C on $t_{\rm on}$ is given by

$$C \ = \ C \ \left(t_{\rm on}\right) = C_0 \ - C_1 \exp\left(-\frac{t_{\rm on}}{C_2}\right). \qquad (7)$$

Based on the empirical model, as depicted by (6) and (7), a function of the starting point of fitting [i.e., $I_{{\rm OFF},D}$ (2.5 μs)] about $t_{\rm on}$ and $t_{\rm off}$ could be obtained. An excellent fitting is achieved between the modeled and the measurement results for various $t_{\rm on}$ and $t_{\rm off}$, as shown in Fig. 7.

D. Influence of the on-State Gate Drive Voltage

For the Schottky-type p-GaN gate HEMT, the p-GaN layer is a "floating region" without a direct electrical connection to any of the transistor's three terminals. Due to the floating nature of p-GaN layer, a drain-bias-induced dynamic positive shift of $V_{\rm TH}$ would occur during switching operation [15], [23]. A sufficiently high V_{GSQ} ($\geq$6 V) is essential to provide an adequate gate overdrive to overcome the $V_{\rm TH}$-shift-induced dynamic $R_{\rm ON}$ degradation in practical switching applications [15]. Meanwhile, with $V_{GSQ} > 5$ V, a high dynamic $I_{\rm OFF}$ induced by the ON-state hole injection could be observed [25]. Because the upper bound of the gate drive voltage is 7 V [26], we develop the dynamic $I_{\rm OFF}$ model with V_{GSQ} in the range of 6 and 7 V.

Dynamic $I_{\rm OFF}$ with dependence on $t_{\rm delay}$ under different V_{GSQ} could be well fitted using (2) [see Fig. 8(a)]. It is found that the time constant τ is the function of V_{GSQ} [see Fig. 8(b)]. As smaller V_{GSQ} results in less injection holes, τ would be smaller with a larger recapturing rate. The fitting function of τ about

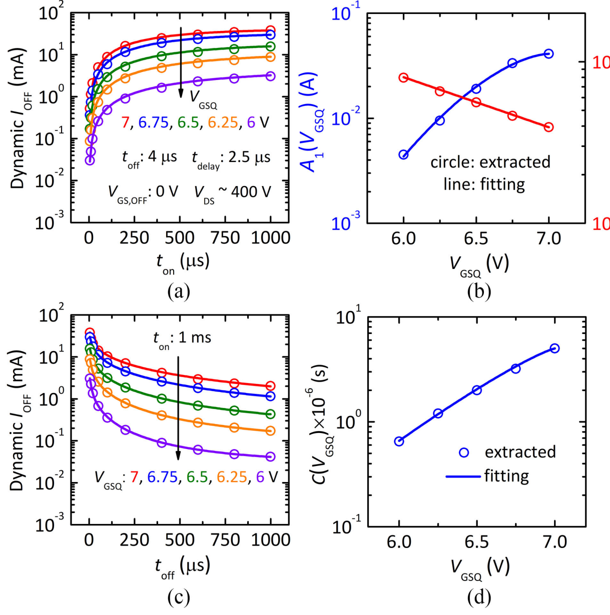

Fig. 9. (a) Dynamic I_{OFF} versus t_{on} with different V_{GSQ}. (b) Extracted parameters of A_1 and B_1 as a function of V_{GSQ}. (c) Dynamic I_{OFF} versus t_{off} with different V_{GSQ}. (d) Extracted parameter of C as a function of V_{GSQ}. The solid lines are fitting curves.

V_{GSQ} is provided as follows:

$$\tau = \tau\ (V_{GSQ}) = \tau\,(7\ \mathrm{V})\exp\left[-\left(\frac{7-V_{GSQ}}{Q_1}\right)^{Q_2}\right]. \quad (8)$$

The impacts of t_{on} and t_{off} on dynamic I_{OFF} with different V_{GSQ} could be well fitted using (5) and (6), respectively [see Fig. 9]. For the dynamic I_{OFF}-t_{on} relation under different V_{GSQ}, as larger V_{GSQ} leads to stronger hole injection into the buffer and deeper penetration depth, more electrons are pumped out of or released from traps, resulting in a higher dynamic I_{OFF} and a larger fitting parameter of A_1. Besides, with a higher V_{GSQ} for more injected holes, dynamic I_{OFF}-t_{on} relation shows a faster speed for its saturation (i.e., A_1), leading to a smaller fitting parameter of B_1. The fitting functions of A_1 and B_1 about V_{GSQ} are given as follows:

$$A_1 = A_1\ (V_{GSQ}) = A_1\ (7\ \mathrm{V})\exp\left[-\left(\frac{7-V_{GSQ}}{Q_3}\right)^{Q_4}\right] \quad (9)$$

$$B_1 = B_1\,(V_{GSQ}) = B_1\ (7\ \mathrm{V})\exp\left[\left(\frac{7-V_{GSQ}}{Q_5}\right)^{Q_6}\right]. \quad (10)$$

The fitting parameter C extracted from Fig. 9(c) is also a function of V_{GSQ}. With a smaller V_{GSQ} results in less injection holes, C would be smaller with a larger recapturing rate. A fitting function of C on V_{GSQ} is given by

$$C = C\ (V_{GSQ}) = C\,(7\ \mathrm{V})\exp\left[-\left(\frac{7-V_{GSQ}}{Q_7}\right)^{Q_8}\right]. \quad (11)$$

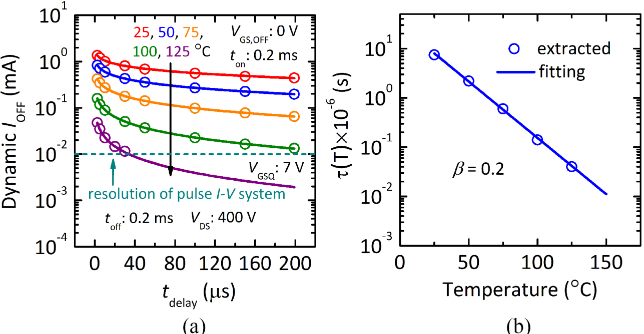

Fig. 10. (a) Dynamic I_{OFF} versus t_{delay} with different temperatures. (b) Extracted time constant τ as a function of temperature. The solid lines are fitting curves.

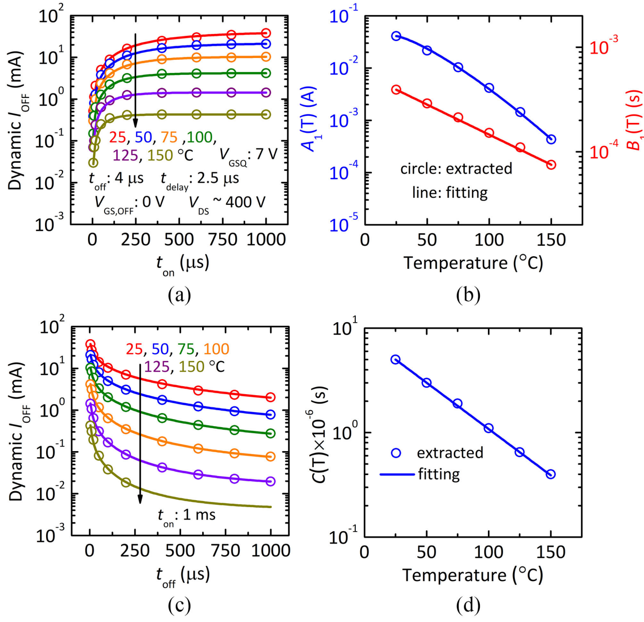

Fig. 11. (a) Dynamic I_{OFF} versus t_{on} with different temperatures. (b) Extracted parameters of A_1 and B_1 as a function of temperature. (c) Dynamic I_{OFF} versus t_{off} with different temperatures. (d) Extracted parameter of C as a function of temperature. The solid lines are fitting curves.

E. Impact of Ambient Temperature

Apart from the various switching conditions, the temperature is also an important impactful factor to dynamic I_{OFF}. In practical switching applications, the power device would operate at a high-voltage/high-current state with high junction temperature. Dynamic I_{OFF} with dependences on t_{delay}, t_{on}, and t_{off} under different temperatures could be well-fitted using (2), (5), and (6), respectively, as shown in Figs. 10 and 11.

The dynamic I_{OFF}-t_{delay} relation under different temperatures and the corresponding time constant τ are plotted in Fig. 10. τ was found to follow an exponential decay function against temperature, as shown in Fig. 10(b), indicating the presence of an activation energy E_a in the process of electrons being recaptured by traps [34]–[36]. After the ON-state hole injection, the ionized traps would recapture electrons injected from the source side of the 2DEG channel. In such a recapturing process, electrons from the source need to overcome an energy barrier to be injected

into the buffer under the gate. Under higher temperatures, more electrons could overcome the barrier to accelerate the recovery process of dynamic I_{OFF} with a smaller τ. The magnitude of E_a can be extracted from the following equation [36]:

$$\tau = \tau_0 \exp\left[\frac{E_a}{kT.}\right] \tag{12}$$

where τ_0 is the limit of decay time at elevated temperature, k is the Boltzmann constant, and T is the ambient temperature (absolute temperature). The calculated E_a is 0.6 eV from the extracted τ in Fig. 10(b) and the fitting function of τ about T is provided as follows:

$$\tau = \tau(T) = \tau(25\,^{\circ}\mathrm{C}) \exp\left[-\left(\frac{T - 25\,^{\circ}\mathrm{C}}{T_1}\right)\right]. \tag{13}$$

For the dynamic I_{OFF}-t_{on} relation under different temperatures [see Fig. 11(a)], the fitting parameter A_1 is smaller with the increase of temperature due to the accelerated electron-recapturing process in the OFF-state with reduced dynamic I_{OFF}. Meanwhile, at elevated temperature, more holes could be injected into the buffer with a higher I_G at the same V_{GSQ} [33]. Dynamic I_{OFF}-t_{on} relation exhibits a faster speed for its saturated level (i.e., A_1), leading to a smaller fitting parameter of B_1. The fitting functions of A_1 and B_1 about T are provided as follows:

$$A_1 = A_1(T) = A_1\ (25\,^{\circ}\mathrm{C}) \exp\left[-\left(\frac{T - 25\,^{\circ}\mathrm{C}}{T_2}\right)^{T_3}\right] \tag{14}$$

$$B_1 = B_1(T) = B_1\ (25\,^{\circ}\mathrm{C}) \exp\left[-\left(\frac{T - 25^{\circ}\mathrm{C}}{T_4}\right)^{T_5}\right]. \tag{15}$$

The fitting parameter C extracted from the dynamic I_{OFF} versus t_{off} curves [see Fig. 11(c)] at higher temperature is smaller owing to the accelerated OFF-state electron-recapturing process. A fitting function of C on T is shown as follows:

$$C = C(T) = C(25\,^{\circ}\mathrm{C}) \exp\left[-\left(\frac{T - 25\,^{\circ}\mathrm{C}}{T_6}\right)^{T_7}\right]. \tag{16}$$

As a result, a model of dynamic I_{OFF} as a function of the OFF-state delay time (t_{delay}), frequency [$f = 1/(t_{\mathrm{on}}+t_{\mathrm{off}})$], duty cycle [$D = t_{\mathrm{on}}/(t_{\mathrm{on}}+t_{\mathrm{off}})$], gate drive voltage ($V_{GSQ}$), and temperature ($T$) is summarized as follows:

$$I_{\mathrm{OFF},\,D}\ (t_{\mathrm{delay}},\ f,\ D,\ V_{GSQ},\ T)$$
$$= \exp\left[-\left(\frac{t_{\mathrm{delay}}}{\tau}\right)^{\beta} + \left(\frac{2.5\ \mu\mathrm{s}}{\tau}\right)^{\beta}\right] * \left[A_1 - A_1 \exp\left(-\frac{D}{fB_1}\right)\right]$$
$$* \left\{\exp\left[-\left(\frac{1-D}{fC}\right)^{D_1} + \left(\frac{4\ \mu\mathrm{s}}{C}\right)^{D_1}\right] \right. \tag{17}$$

where

$$\tau = \tau\ (f,\ D,\ V_{GSQ},\ T) = \left[\tau_0 - \tau_1 \exp\left(-\frac{D}{f\tau_2}\right)\right]$$
$$* \exp\left[-\left(\frac{7 - V_{GSQ}}{Q_1}\right)^{Q_2}\right] * \exp\left[-\left(\frac{T - 25\,^{\circ}\mathrm{C}}{T_1}\right)\right]$$

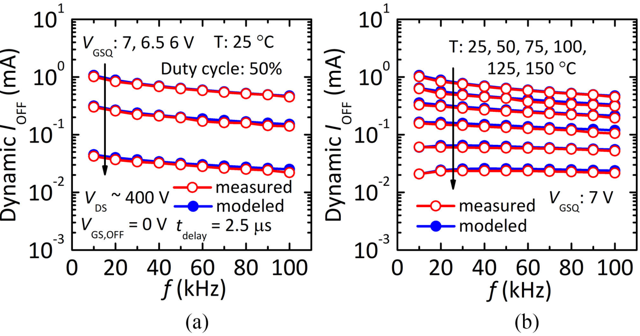

Fig. 12. Modeled and measured dynamic I_{OFF} versus frequency with different (a) V_{GSQ} and (b) temperatures.

$$A_1 = A_1(V_{GSQ},\ T) = A_1(7\ \mathrm{V},\ 25\,^{\circ}\mathrm{C})$$
$$* \exp\left[-\left(\frac{7 - V_{GSQ}}{Q_3}\right)^{Q_4}\right] * \exp\left[-\left(\frac{T - 25\,^{\circ}\mathrm{C}}{T_2}\right)^{T_3}\right]$$

$$B_1 = B_1(V_{GSQ},\ T) = B_1(7\ \mathrm{V},\ 25\,^{\circ}\mathrm{C})$$
$$* \exp\left[\left(\frac{7 - V_{GSQ}}{Q_5}\right)^{Q_6}\right] * \exp\left[-\left(\frac{T - 25\,^{\circ}\mathrm{C}}{T_4}\right)^{T_5}\right]$$

$$C = C\ (f,\ D,\ V_{GSQ},\ T) = \left[C_0 - C_1 \exp\left(-\frac{D}{fC_2}\right)\right]$$
$$* \exp\left[-\left(\frac{7 - V_{GSQ}}{Q_7}\right)^{Q_8}\right] * \exp\left[-\left(\frac{T - 25^{\circ}\mathrm{C}}{T_6}\right)^{T_7}\right]$$

$$t_{\mathrm{on}} = \frac{D}{f},\ t_{\mathrm{off}} = \frac{1-D}{f},\ (6\ \mathrm{V} \le V_{GSQ} \le 7\ \mathrm{V}).$$

IV. Results and Discussion

According to (17), the modeled dynamic I_{OFF} versus frequency under different V_{GSQ} and temperature with $V_{GS,\mathrm{OFF}} = 0$ V, $V_{DS} \sim 400$ V, $t_{\mathrm{delay}} = 2.5\ \mu$s, and duty cycle = 50% is calculated in Fig. 12 with the corresponding measurement results. The modeled results could agree well with the experimental data.

Also, by using the closed-form empirical model of dynamic I_{OFF}, the dynamic I_{OFF} induced OFF-state power consumption $E_{\mathrm{OFF},D}$ in each cycle can be calculated. For any given switching conditions with a certain switching frequency, duty cycle, gate drive voltage, and temperature, dynamic I_{OFF} in each cycle is the function of time [$I_{\mathrm{OFF},D}\ (t)$], following the dynamic I_{OFF}-t_{delay} relation. The $E_{\mathrm{OFF},D}$ could be calculated by integrating $I_{\mathrm{OFF},D}\ (t)$ during the OFF-state time ($t_{\mathrm{off}} = (1-D)/f$) and then multiplying by V_{DS}, as follows:

$$E_{\mathrm{OFF},D} = V_{DS} * \int_0^{\frac{1-D}{f}} I_{\mathrm{OFF},D}\ (t)\ dt. \tag{18}$$

The static E_{OFF} ($E_{\mathrm{OFF},S}$) and the ON-state power consumption, E_{ON} can be calculated as follows:

$$E_{\mathrm{OFF},S} = V_{DS} * I_{\mathrm{OFF},S} * \frac{1-D}{f} \tag{19}$$

$$E_{\mathrm{ON}} = I_{\mathrm{ON}}{}^2 * R_{\mathrm{ON},D} * \frac{D}{f}. \tag{20}$$

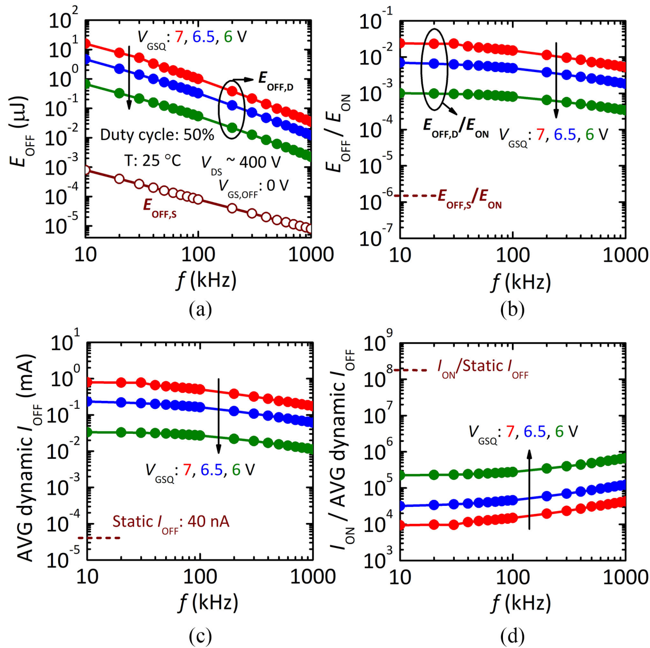

Fig. 13. Modeled (a) $E_{\rm OFF}$, (b) $E_{\rm OFF}/E_{\rm ON}$ ratio, (c) average dynamic $I_{\rm OFF}$, and (d) $I_{\rm ON}$/average dynamic $I_{\rm OFF}$ ratio versus frequency with different V_{GSQ} under room temperature. The corresponding static OFF-state characteristics are also calculated.

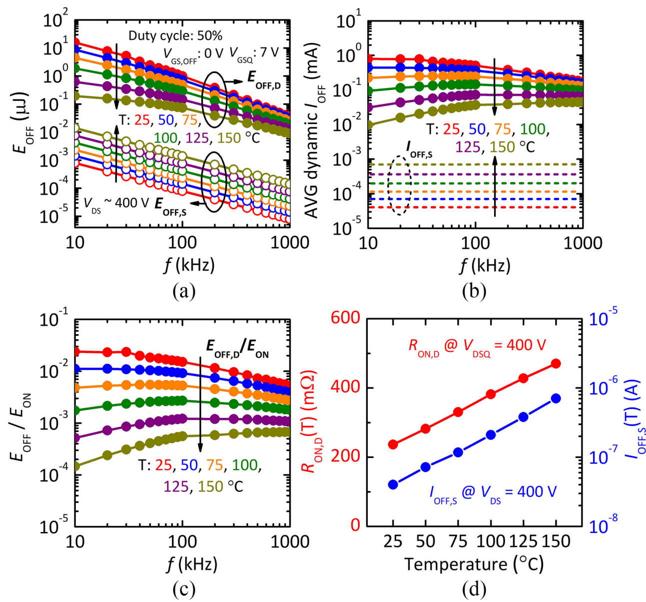

Fig. 14. Modeled (a) $E_{\rm OFF}$, (b) average dynamic $I_{\rm OFF}$, and (c) $E_{\rm OFF}/E_{\rm ON}$ ratio versus frequency with different ambient temperatures. (d) $R_{{\rm ON},D}$ and $I_{{\rm OFF},S}$ versus temperature. The corresponding static OFF-state characteristics are also calculated.

For the 650-V/7.5-A p-GaN gate HEMT, the $I_{\rm ON}$ is set to be 7.5 A for the ON-state loss calculation and $R_{{\rm ON},D}$ is the dynamic $R_{\rm ON}$ measured by a pulsed I--V system with a quiescent drain bias (V_{DSQ}) of 400 V. Under room temperature, the dynamic $I_{\rm OFF}$ induced $E_{\rm OFF}$ ($E_{{\rm OFF},D}$), $E_{{\rm OFF},D}/E_{\rm ON}$ ratio, average (AVG) dynamic $I_{\rm OFF}$ in the OFF-state, and $I_{\rm ON}$/AVG dynamic $I_{\rm OFF}$ ratio are calculated from 10 kHz to 1 MHz with a duty cycle of 50% and different V_{GSQ}, as shown in Fig. 13. With the p-GaN gate HEMT operating at the high switching frequency of 1 MHz with the gate drive voltage from 6 to 7 V, the $I_{\rm ON}$/AVG dynamic $I_{\rm OFF}$ ratio is calculated from 6.7×10^5 to 4.3×10^4, which is two to three orders of magnitude lower than the $I_{\rm ON}$/static $I_{\rm OFF}$ ratio. The higher dynamic $I_{\rm OFF}$ leads to a larger $E_{\rm OFF}$. The $E_{{\rm OFF},D}/E_{\rm ON}$ ratio is calculated from 0.034% to 0.53% with V_{GSQ} from 6 to 7 V at 1 MHz, indicating sufficiently low OFF-state power consumption. If the switching frequency is lower at 100 kHz, the $E_{{\rm OFF},D}/E_{\rm ON}$ ratio increases to 1.5% at a V_{GSQ} of 7 V, suggesting that the OFF-state power loss should be taken into account in the power efficiency estimation.

The temperature-dependent results are calculated and summarized in Fig. 14. At higher temperature, electron mobility becomes smaller and $R_{{\rm ON},D}$ would increase with a higher $E_{\rm ON}$ [see Fig. 14(d)]. An increase in temperature could enhance electron emission over the energy barrier in the leakage path, resulting in the increase of static $I_{\rm OFF}$ ($I_{{\rm OFF},S}$). Meanwhile, the electron-recapturing process in the OFF-state at higher temperatures would be accelerated, facilitating the recovery process of dynamic $I_{\rm OFF}$ with reduced $E_{{\rm OFF},D}$ [see Fig. 14(a)].

Unlike the AVG dynamic $I_{\rm OFF}$ in the OFF-state at room temperature, which is negatively correlated with frequency due to the decreased ON-state duration time ($t_{\rm on}$) with weaker hole injection in each cycle, the AVG dynamic $I_{\rm OFF}$ at high temperature (e.g., 150 °C) would show a positive correlation to frequency [see Fig. 14(b)]. At a higher temperature, the OFF-state carrier-recapturing process is enhanced. With the increase of frequency at a duty cycle of 50%, the shorter OFF-state time ($t_{\rm off}$) in each cycle with a weaker electron-recapturing process would become the dominant factor, leading to the increase of AVG dynamic $I_{\rm OFF}$. With the p-GaN gate HEMT operating at a gate drive voltage of 7 V and a high temperature of 150 °C, the AVG dynamic $I_{\rm OFF}$ is about two orders of magnitude higher than the static $I_{\rm OFF}$, and the $E_{{\rm OFF},D}/E_{\rm ON}$ ratio is calculated to be 0.06%–0.07% with the frequency from 100 kHz to 1 MHz [see Fig. 14(c)], indicating that a high junction temperature in real applications for the p-GaN gate HEMTs has a positive effect on the reduction of dynamic $I_{\rm OFF}$.

TABLE II
VALUES OF FITTING PARAMETERS EMPLOYED IN (17)

A_1 (7 V, 25 °C)	B_1 (7 V, 25 °C)	A_2	
0.041 A	3.9321×10^{-4} s	0.009	
τ_0	τ_1	τ_2	
1.8925×10^{-5} s	1.8624×10^{-5} s	4.0433×10^{-4} s	
C_0	C_1	C_2	D
2.0388×10^{-5} s	1.9984×10^{-5} s	0.00486 s	0.265
Q_1	Q_2	Q_3	Q_4
0.66 V	1.6	0.61 V	1.64
Q_5	Q_6	Q_7	Q_8
1.4 V	1	0.55 V	1.18
T_1	T_2	T_3	T_4
19 °C	39 °C	1.3	75.5 °C
T_5	T_6	T_7	β
1	49 °C	1	0.2

The corresponding values of fitting parameters in (17) used for the calculation of power loss are given in Table II. The fitting parameters are extracted using the Origin software by Chi-Square method with minimum standard error. For the dynamic $I_{\rm OFF}$ issue in other types of p-GaN gate HEMTs, the

fitting parameters in (17) could be tuned to model devices manufactured by different companies.

It should be noted that applying a sufficiently large negative gate turn-OFF voltage (e.g., $V_{GS,\mathrm{OFF}} \leq$ -3 V) is an effective strategy to minimize the dynamic I_{OFF} and E_{OFF} in practical switching applications [25]. However, the negative $V_{GS,\mathrm{OFF}}$ does have an adverse effect in which it would raise the HEMT device's reverse turn-ON voltage ($V_{R\text{-}T}$) that results in larger reverse conduction loss, as $V_{R\text{-}T}$ is determined by $V_{GS,\mathrm{OFF}}$ and V_{TH} ($V_{R\text{-}T} = |V_{GS,\mathrm{OFF}} - V_{\mathrm{TH}}|$). To eliminate such larger reverse conduction loss induced by negative $V_{GS,\mathrm{OFF}}$, an integrated antiparallel diode can be implemented. For example, a *p*-GaN gate HEMT with distributed built-in Schottky barrier diode (SBD) has been recently developed with a good balance between the forward and reverse conduction [38]. The built-in SBD provides a low reverse turn-ON voltage, which is independent of the V_{TH} and $V_{GS,\mathrm{OFF}}$. Besides, this device exploits the common access region in both forward conduction and reverse conduction; thus, an area-efficient solution with minimized reverse conduction loss could be achieved.

V. Conclusion

A physics-based empirical model of dynamic I_{OFF} under switching operation in *p*-GaN gate HEMT is established by the considerations of switching frequency, duty cycle, OFF-state delay time, ON-state gate drive voltage, and temperature. The modeled dynamic I_{OFF} shows a good agreement with the measurement results. By using this model, the corresponding OFF-state power consumption and OFF/ON-state power consumption ratio under dynamic operation could be accurately estimated in applications featuring different switching conditions, providing valuable guidance to evaluate the impact of dynamic I_{OFF}.

References

[1] K.-Y. R. Wong *et al.*, "A next-generation CMOS-compatible GaN-on-Si transistors for high efficiency energy systems," in *Proc. IEEE Int. Electron Devices Meeting*, Washington, DC, USA, Dec. 2015, pp. 9.5.1–9.5.4.

[2] Y. Wu, M. Jacob-Mitos, M. L. Moore, and S. Heikman, "A 97.8% efficient GaN HEMT boost converter with 300-W output power at 1 MHz," *IEEE Electron Device Lett.*, vol. 29, no. 8, pp. 824–826, Aug. 2008.

[3] K. J. Chen *et al.*, "GaN-on-Si power technology: Devices and applications," *IEEE Trans. Electron Devices*, vol. 64, no. 3, pp. 779–795, Mar. 2017.

[4] Y. Cai, Y. Zhou, K. M. Lau, and K. J. Chen, "Control of threshold voltage of AlGaN/GaN HEMTs by fluoride-based plasma treatment: From depletion mode to enhancement mode," *IEEE Trans. Electron Devices*, vol. 53, no. 9, pp. 2207–2215, Sep. 2006.

[5] X. Hu, G. Simin, J. Yang, M. A. Khan, R. Gaska, and M. S. Shur, "Enhancement mode AlGaN/GaN HFET with selectively grown pn junction gate," *Electron. Lett.*, vol. 36, no. 8, pp. 753–754, Apr. 2000.

[6] K. J. Chen and C. Zhou, "Enhancement-mode AlGaN/GaN HEMT and MIS-HEMT technology," *Phys. Status Solidi A*, vol. 208, no. 2, pp. 434–438, Feb. 2011.

[7] M. Hua *et al.*, "Integration of LPCVD-SiN_X gate dielectric with recessed-gate E-mode GaN MIS-FETs: Toward high performance, high stability and long TDDB lifetime," in *Proc. IEEE Int. Electron Devices Meeting*, San Francisco, CA, USA, Dec. 2016, pp. 10.4.1–10.4.4.

[8] D. Reusch, J. Strydom, and A. Lidow, "A new family of GaN transistors for highly efficient high frequency dc-dc converters," in *Proc. IEEE Appl. Power Electron. Conf. Expo.*, Mar. 2015, pp. 1979–1985.

[9] M. Ishida, T. Ueda, T. Tanaka, and D. Ueda, "GaN on Si technologies for power switching devices," *IEEE Trans. Electron Devices*, vol. 60, no. 10, pp. 3053–3059, Oct. 2013.

[10] C.-L. Tsai *et al.*, "Smart GaN platform: Performance & challenges," in *Proc. IEEE Int. Electron Devices Meeting*, San Francisco, CA, USA, Dec. 2017, pp. 33.1.1–33.1.4.

[11] Y. Uemoto *et al.*, "Gate injection transistor (GIT): A normally-off AlGaN/GaN power transistor using conductivity modulation," *IEEE Trans. Electron Devices*, vol. 54, no. 12, pp. 3393–3399, Dec. 2007.

[12] S. Kaneko *et al.*, "Current-collapse-free operations up to 850 V by GaN-GIT utilizing hole injection from drain," in *Proc. IEEE 27th Int. Symp. Power Semicond. Devices IC's*, May 2015, pp. 41–44.

[13] K. Tanaka *et al.*, "Reliability of hybrid-drain-embedded gate injection transistor," in *Proc. IEEE Int. Rel. Phys. Symp.*, Apr. 2017, pp. 4B-2.1–4B-2.10.

[14] M. Meneghini, O. Hilt, J. Wuerfl, and G. Menehesso, "Technology and reliability of normally-off GaN HEMTs with p-type gate," *Energies*, vol. 10, no. 2, pp. 1–15, Jan. 2017.

[15] H. Wang, J. Wei, R. Xie, C. Liu, G. Tang, and K. J. Chen, "Maximizing the performance of 650-V p-GaN HEMTs: Dynamic R_{ON} characterization and circuit design considerations," *IEEE Trans. Power Electron.*, vol. 32, no. 7, pp. 5539–5549, Jul. 2017.

[16] I. Hwang *et al.*, "p-GaN gate HEMTs with tungsten gate metal for high threshold voltage and low gate current," *IEEE Electron Device Lett.,* vol. 34, no. 2, pp. 202–204, Feb. 2013.

[17] T. Wu *et al.*, "Forward bias gate breakdown mechanism in enhancement-mode p-GaN gate AlGaN/GaN high-electron mobility transistors," *IEEE Electron Device Lett.*, vol. 36, no. 10, pp. 1001–1003, Oct. 2015.

[18] A. N. Tallarico *et al.*, "Investigation of the p-GaN gate breakdown in forward-biased GaN-based power HEMTs," *IEEE Electron Device Lett.*, vol. 38, no. 1, pp. 99–102, Jan. 2017.

[19] S. Huang, Q. Jiang, S. Yang, C. Zhou, and K. J. Chen, "Effective passivation of AlGaN/GaN HEMTs by ALD-grown AlN thin film," *IEEE Electron Device Lett.*, vol. 33, no. 4, pp. 516–518, Apr. 2012.

[20] S. Huang, Q. Jiang, S. Yang, Z. Tang, and K. J. Chen, "Mechanism of PEALD-grown AlN passivation for AlGaN/GaN HEMTs: Compensation of interface traps by polarization charges," *IEEE Electron Device Lett.*, vol. 34, no. 2, pp. 193–195, Feb. 2013.

[21] S. Karmalkar and U. K. Mishra, "Enhancement of breakdown voltage in AlGaN/GaN high electron mobility transistors using a field plate," *IEEE Trans. Electron Devices*, vol. 48, no. 8, pp. 1515–1521, Aug. 2001.

[22] M. J. Uren *et al.*, "Leaky dielectric" mode for the suppression of dynamic R_{ON} in carbon-doped AlGaN/GaN HEMTs," *IEEE Trans. Electron Devices*, vol. 64, no. 7, pp. 2826–2834, Jul. 2017.

[23] J. Wei *et al.*, "Charge storage mechanism of drain induced dynamic threshold voltage shift in *p*-GaN gate HEMTs," *IEEE Electron Device Lett.*, vol. 40, no. 4, pp. 526–529, Apr. 2019.

[24] Y. Wang *et al.*, "Dynamic OFF-state current (dynamic I_{OFF}) in *p*-GaN gate HEMTs with an Ohmic gate contact," *IEEE Electron Device Lett.*, vol. 39, no. 9, pp. 1366–1369, Sep. 2018.

[25] Y. Wang, J. Wei, S. Yang, J. Lei, M. Hua, and K. J. Chen, "Investigation of dynamic I_{OFF} under switching operation in Schottky-type p-GaN gate HEMTs," *IEEE Trans. Electron Devices*, vol. 66, no. 9, pp. 3789–3794, Sep. 2019.

[26] GaN Systems, GS66502B Datasheet. 2018. [Online]. Available: http://gansystems.com/wp-content/uploads/2018/04/GS66502B-DS-Rev-180420.pdf

[27] G. Tang *et al.*, "High capacitance-density *p*-GaN gate capacitors for high-frequency power integration," *IEEE Electron Device Lett.,* vol. 39, no. 9, pp. 1362–1365, Sep. 2018.

[28] X. Tang, B. Li, H. A. Moghadam, P. Tanner, J. Han, and S. Dimitrijev, "Mechanism of threshold voltage shift in p-GaN gate AlGaN/GaN transistors," *IEEE Electron Device Lett.*, vol. 39, no. 8, pp. 1145–1148, Aug. 2018.

[29] C. Zhou, Q. Jiang, S. Huang, and K. J. Chen, "Vertical leakage/breakdown mechanisms in AlGaN/GaN-on-Si devices," *IEEE Electron Device Lett.,* vol. 33, no. 8, pp. 1132–1134, Aug. 2012.

[30] E. Bahat-Treidel, F. Brunner, O. Hilt, E. Cho, J. Würfl, and G. Tränkle, "AlGaN/GaN/GaN: C back-barrier HFETs with breakdown voltage of over 1 kV and low $R_{\mathrm{ON}} \times A$," *IEEE Trans. Electron Devices*, vol. 57, no. 11, pp. 3050–3058, Nov. 2010.

[31] A. Rizzo, G. Micocci, and A. Tepore, "Space-charge-limited currents in insulators with two sets of traps distributed in energy: Theory and experiment," *J. Appl. Phys.*, vol. 48, no. 8, pp. 3415–3424, Aug. 1977.

[32] B. Li, H. Li, J. Wang, and X. Tang, "Asymmetric bipolar injection in a Schottky-metal/*p*-GaN/AlGaN/GaN device under forward bias," *IEEE Electron Device Lett.,* vol. 40, no. 9, pp. 1389–1392, Sep. 2019.

[33] X. Tang, R. Qiu, Y. Liu, and B. Li, "Thermally enhanced hole injection and breakdown in a Schottky-metal/*p*-GaN/AlGaN/GaN device under forward bias," *Appl. Phys. Lett.*, vol. 117, no. 4, pp. 043501-1–043501-5, Jul. 2020.
[34] B. Li, Q. Jiang, S. Liu, C. Liu, and K. J. Chen, "Degradation of transient OFF-state leakage current in AlGaN/GaN HEMTs induced by ON-state gate overdrive," *Phys. Status Solidi C*, vol. 11, no. 3/4, pp. 928–931, Feb. 2014.
[35] X. Tang, B. Li, H. A. Moghadam, P. Tanner, J. Han, and S. Dimitrijev, "Effect of hole-injection on leakage degradation in a p-GaN gate AlGaN/GaN power transistor," *IEEE Electron Device Lett.*, vol. 39, no. 8, pp. 1203–1206, Aug. 2018.
[36] H. M. Chen, Y. F. Chen, M. C. Lee, and M. S. Feng, "Persistent photoconductivity in n-type GaN," *J. Appl. Phys.*, vol. 82, no. 2, pp. 899–901, Apr. 1997.
[37] J. L. Lyons, A. Janotti, and C. G. van de Walle, "Effects of carbon on the electrical and optical properties of InN, GaN, and AlN," *Phys. Rev. B*, vol. 89, no. 3, pp. 035204-1–035204-8, Jan. 2014.
[38] L. Zhang *et al.*, "*p*-GaN power transistor with distributed built-in Schottky-barrier diode for low-loss reverse conduction," *IEEE Electron Device Lett.*, vol. 41, no. 3, pp. 341–344, Mar. 2020.

Yuru Wang received the B.S. degree in electronic science and technology (microelectronic technology) and the M.S. degree in microelectronics and solid-state electronics from the University of Electronic Science and Technology of China, Chengdu, China, in 2013 and 2016, respectively, and the Ph.D. degree in electronic and computer engineering from The Hong Kong University of Science and Technology, Hong Kong, in 2020.

Tao Chen received the B.S. degree in microelectronics science and engineering from the University of Electronic Science and Technology of China, Chengdu, China, in 2019. He is currently working toward the Ph.D. degree in electronic and computer engineering with The Hong Kong University of Science and Technology, Hong Kong.

Mengyuan Hua (Member, IEEE) received the B.S. degree in mathematics and physics (basic class) from Tsinghua University, Beijing, China, and the Ph.D. degree in electronic and computer engineering from The Hong Kong University of Science and Technology, Hong Kong, in 2013 and 2017, respectively.

She is currently an Assistant Professor with the Department of Electric and Electronic Engineering, Southern University of Science and Technology, Shenzhen, China.

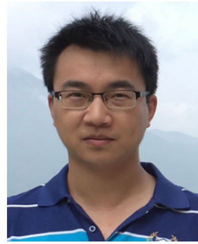

Jin Wei (Member, IEEE) received the B.S. degree in microelectronics from Sun Yat-sen University, Guangzhou, China, in 2010, the M.S. degree in microelectronics and solid-state electronics from the University of Electronic Science and Technology of China, Chengdu, China, in 2013, and the Ph.D. degree in electronic and computer engineering from The Hong Kong University of Science and Technology, Hong Kong, in 2017.

He is currently an Assistant Professor with the Institute of Microelectronics, Peking University, Beijing, China.

Zheyang Zheng received the B.S. degree in electronic science and engineering from Zhejiang University, Hangzhou, China, in 2016. He is currently working toward the Ph.D. degree in electronic and computer engineering with The Hong Kong University of Science and Technology, Hong Kong.

Wenjie Song received the B.S. degree in microelectronics and solid-state electronics from Xi'an Jiaotong University, Xi'an, China, in 2013. He is currently working toward the Ph.D. degree in electronic and computer engineering with The Hong Kong University of Science and Technology, Hong Kong.

Song Yang received the B.S. degree in electronic science and technology from Xi'an Jiaotong University, Xi'an, China, in 2013, and the Ph.D. degree in electronic and computer engineering from The Hong Kong University of Science and Technology, Hong Kong, in 2020.

Kailun Zhong received the B.S. degree in microelectronics and solid-state electronics from the University of Electronic Science and Technology of China, Chengdu, China, in 2017. He is currently working toward the Ph.D. degree in electronic and computer engineering with The Hong Kong University of Science and Technology, Hong Kong.

Kevin J. Chen (Fellow, IEEE) received the B.S. degree in electronics from Peking University, Beijing, China, and the Ph.D. degree in physics from the University of Maryland, College Park, MD, USA, in 1988 and 1993, respectively.

He has obtained industry experience by conducting R&D work on III-V high-speed device technologies with NTT LSI Laboratories, Japan, and Agilent Technologies, USA. In 2000, he joined The Hong Kong University of Science and Technology, Hong Kong, where he is currently a Professor with the Department of Electronics and Computer Engineering. He has authored or coauthored more than 450 publications in international journals and conference proceedings, and has been granted 12 U.S. patents on GaN electron device technologies. His research is currently focused on developing wide-bandgap semiconductor device technologies for high-power and high-frequency applications.

Dr. Chen is currently an Editor for the IEEE TRANSACTIONS ON ELECTRON DEVICES, and was an Editor for the IEEE TRANSACTIONS ON MICROWAVE THEORY AND TECHNIQUES and *Japanese Journal of Applied Physics*. He was the Technical Program Chair of the International Symposium on Power Semiconductor Devices and ICs in 2019.